Monte-Carlo Simulations for the optimisation of a TOF-MIEZE Instrument

T. Weber[a,b], G. Brandl[a,b], R. Georgii[a,b], W. Häußler[a,b], S. Weichselbaumer[a], P. Böni[b]

[a]*Forschungsneutronenquelle Heinz Maier-Leibnitz, Technische Universität München, Lichtenbergstr. 1, 85748 Garching, Germany*
[b]*Physik Department E21, Technische Universität München, James-Franck-Str., 85748 Garching, Germany*

Abstract

The MIEZE (Modulation of Intensity with Zero Effort) technique is a variant of neutron resonance spin echo (NRSE), which has proven to be a unique neutron scattering technique for measuring with high energy resolution in magnetic fields. Its limitations in terms of flight path differences have already been investigated analytically for neutron beams with vanishing divergence. In the present work Monte-Carlo simulations for quasi-elastic MIEZE experiments taking into account beam divergence as well as the sample dimensions are presented. One application of the MIEZE technique could be a dedicated NRSE-MIEZE instrument at the European Spallation Source (ESS) in Sweden. The optimisation of a particular design based on Montel mirror optics with the help of Monte Carlo simulations will be discussed here in detail.

Keywords: MIEZE, spin echo, Monte Carlo Simulation, MISANS, ESS

1. Introduction

One major field of current solid state physics is complex magnetic systems. Examples are the structure and dynamics of topological spin structures like skyrmions in metals, semiconductors and ferroelectric insulators [1, 2, 3, 4]. Others are the dynamics of spin waves in ferromagnets like EuO and Fe [5]. Further interest focuses on the slow magnetic dynamics of magnetic monopoles and Dirac strings in spin ice [6]. Generally, excitations with lifetimes from the picosecond to the microsecond range near quantum phase transitions are of utmost interest for the understanding of the magnetic dynamics in complex materials, especially with regard to possible applications in spintronics.

The standard technique to measure quasi-elastic dynamics in the higher ps and ns time range is Neutron Spin Echo (NSE) [7]. As a Larmor precession technique it is sensitive to magnetic fields and can only be used with magnetic fields at the sample position by applying rather complicated spin manipulation resulting in a loss of intensity [5]. The complementary Neutron Resonance Spin Echo (NRSE) method invented by Golub and Gähler [8, 9] shares the sensitivity to magnetic fields or depolarising samples, but can be evolved straightforwardly into the MIEZE technique [9, 10, 11], which is then independent of sample depolarisation effects, as all spin manipulations are performed before the sample.

As MIEZE is effectively a time-of-flight method it is sensitive to differences in the length of the neutron flight path. This drawback has been studied analytically in reference [12] for beams with zero divergence. But for analysing MIEZE data and designing MIEZE instruments the effect of divergence and the influence of the neutron path on the resolution is required.

In this study we will show that using the Monte Carlo simulation package McStas [13, 14] together with specifically written components for the MIEZE setup, both earlier analytical and experimental results can be reproduced and furthermore be used to assess the suitability of more elaborate instrument designs. MIEZE is an excellent technique for high energy resolution measurements: For small samples spin-echo times of the order of a microsecond are possible with currently available components such as RF spin flipper coils and TOF detectors.

2. MIEZE technique

As a variant of NRSE, the MIEZE technique omits both π-flipper coils after the sample [9]. The coils before the sample are separated by a distance L_1 and are driven at two different frequencies, $\omega_1 < \omega_2$. After passing the RF-flippers, which are working in resonant π-flip mode without bootstrap, the neutron spin phase depends on the flight time and the neutron velocity v. At a distance L_2 given by

$$\omega_1 \cdot L_1 = (\omega_2 - \omega_1) \cdot L_2 \tag{1}$$

the spin modulation of all velocity groups adds up in phase. Eq. (1) is called the MIEZE condition. The key point of MIEZE is now that the spin modulation can be converted to an intensity modulation by placing a polariser anywhere after the second coil, in particular before the sample. Then a time-resolved detector is required, which registers a sinusoidally modulated signal of the frequency ω_M $I(t) \propto \cos(\omega_M t)$, where $\omega_M = 2(\omega_2 - \omega_1)$ is the MIEZE frequency.

If the phase at the detector is not uniform, which can be caused by inelastic scattering at the sample or by path length differences after the polariser, the modulation is damped and the signal can be described by $I(t) = B + A \cos(\omega_M t)$. For negligible path length differences the MIEZE contrast $C = A/B$

is a measure of the inelasticity of the scattering, which is the MIEZE equivalent of the measured polarisation in NSE/NRSE.

It can be shown [15] that with an ideal setup, the contrast is the cosine Fourier transform of the scattering law $S(q, \omega)$ of the sample

$$C(q, \tau_M) = \int d\omega\, S(q, \omega)\, \cos(\omega \tau_M), \tag{2}$$

with the sample placed at the position L_S before the detector. With m being the mass of the neutron, the MIEZE time τ_M is given by

$$\tau_M = \frac{\hbar \omega_M L_S}{m v^3}, \tag{3}$$

This is the Fourier time of the instrument, equivalent to the spin-echo time of NSE/NRSE [15].

For a real MIEZE instrument, the contrast of the modulation is reduced by imperfections of polarisers, coils, detector and by path length differences. The reduction in contrast C due to different sample shapes and spin-echo times was studied theoretically in reference [12]. To benchmark the quality of the Monte-Carlo simulation of MIEZE, we reproduce and verify the previous work in the next section.

3. MIEZE and Monte-Carlo simulations

3.1. Reproduction of previous results

For the reproduction of the previous results from the reference [12] we used the Monte-Carlo simulation package McStas [13, 14] simulating a standard MIEZE setup without any additional neutron optics and the sample only.

The contrast of the MIEZE signal is reduced by several effects of which we discuss the most important ones, namely the thickness of the absorber in the detectors, the resolution of the detector and the geometry of the sample in more detail. The effect of imperfections in the NRSE coils on the spin and the dependence on the MIEZE frequency ω_M is not taken into account here as the coils are simulated as ideal RF spin flippers.

The thickness Δd of the detector modifies the registered contrast by introducing a phase shift in equation (2)

$$C = \frac{1}{\Delta d} \int d\omega \int_0^{\Delta d} dx\, S(\omega) \cos(\omega \tau_M + \omega_M x/v). \tag{4}$$

A phase shift of 2π over the whole thickness of the detector would completely destroy the contrast, whereas a phase shift of $\pi/2$ would not reduce it by more than 10 %. For example in the CASCADE detector [16, 17, 18] we used in our MIEZE experiments, where the thickness of the detection planes is $\Delta d = 2\,\mu m$, a 10 % loss of contrast happens at MIEZE frequencies of $\omega_M = 621\,\text{MHz}$, $\omega_M = 311\,\text{MHz}$ and $\omega_M = 207\,\text{MHz}$ for $\lambda = 5\,\text{Å}$, $\lambda = 10\,\text{Å}$ and $\lambda = 15\,\text{Å}$, respectively. For the respective wavelengths this corresponds to a maximum possible MIEZE time of $\tau_M = 1\,\mu s$, $\tau_M = 4\,\mu s$ and $\tau_M = 9\,\mu s$, which is far above the values considered here (see Figures 6 and 7) thus justifying the assumption of a thin detector in the simulations.

To counter the effect of contrast reduction due to path length differences within the plane of the detector especially at higher

MIEZE times τ_M an area of $1\,mm^2$ is used in the simulation. This is in the order of the spatial resolution of a CASCADE detector.

As the thickness and spatial resolution of the detector therefore do not contribute significantly to the contrast reduction, we only have to consider the reduction factor due to the sample in the following.

In the simulations the contrast is normalised to its value at $q = 0$. Vanadium is used as a purely elastic scatterer. Fig. 1 shows a comparison of the simulated and calculated [12] reduction factors due to different sample shapes in fixed and reflecting geometry (where reflecting is defined as a rotation $\phi = \theta/2 - 90°$ in the direction of θ, see Fig. 1) For the spherical and cylindrical samples absorption is neglected. This simplification is necessary because the analytical formulae in [12] do not take into account the additional contrast reduction caused by inhomogeneous absorption due to sample shape. The results demonstrate an almost perfect agreement between the analytical and the simulated results.

Fig. 2 shows the simulated (solid lines), calculated (dashed lines) and measured (symbols with error bar) reduction factors for a cuboid sample in fixed geometry for different spin-echo times τ_M. There is an excellent agreement between simulation (this work), calculation and measurement (from [12]).

Summarising, the effects of contrast reduction due to the geometry of the sample calculated using an analytical method are very well reproduced by the McStas simulations using a standard MIEZE setup with no additional neutron optics (compare Figs. 1 and 2 in this paper to Figs. 6 and 7 in [12]).

3.2. Compensation for detector misalignment

In a real experiment with a total length in the order of several tens of metres a detector misalignment relative to the coils violating the MIEZE condition, will lead to a reduction of MIEZE contrast. We briefly show that this effect can easily be compensated by adjusting one of the RF frequencies.

A detector that is misaligned by an offset of Δl away from L_2 does not fulfill the MIEZE condition (Eq. 1) anymore. However, the signal can be recovered by adjusting the frequency of one of the π-flipper coils. This can immediately be seen if we substitute L_2 by $L_2 + \Delta l$ and ω_1 by $\omega_1 + \Delta\omega_1$ in eq. (1) and solve for $\Delta\omega_1$:

$$\Delta\omega_1 = (\omega_2 - \omega_1) - \frac{L_1 \cdot \omega_2}{\Delta l + L_1 + L_2} \tag{5}$$

According to Eq. (5), the first spin flipper frequency ω_1 has to be adjusted by $\Delta\omega_1$ to compensate for a detector misalignment of Δl. The simulations (Fig. 3) show that the signal can be perfectly recovered.

4. A dedicated NRSE-MIEZE instrument at the ESS

In the following we show how the newly developed simulation tools can be used to demonstrate the feasibility of a focusing MIEZE beam line for various q and τ_M parameters.

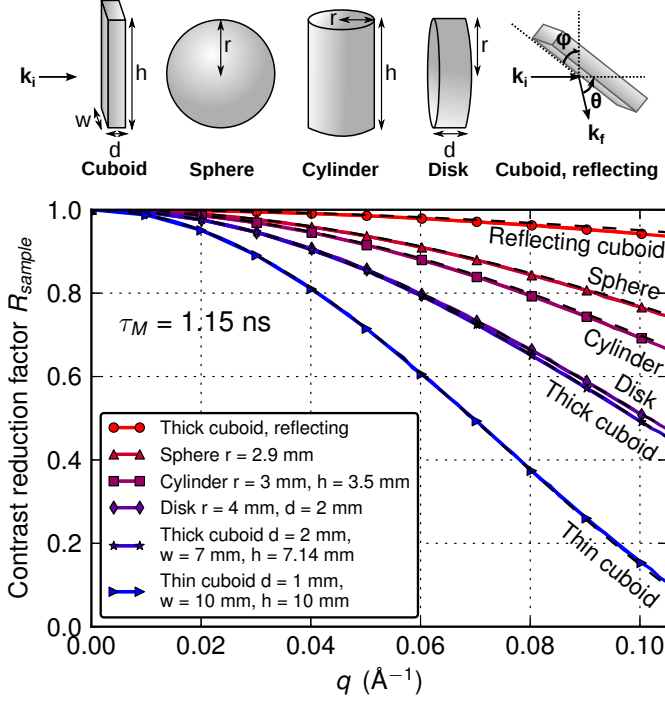Figure 1: Top: The different sample shapes are shown. In the reflecting geometry the sample is rotated at an angle $\phi = \theta/2 - 90°$ with respect to the scattering angle as indicated in the figure. Bottom: Comparison of the sample reduction factor for different geometries with constant sample volume $V = 100\ \text{mm}^3$ using the analytical results from [12] (dashed lines) and simulated results (solid lines). Parameters are as given in [12]: $\omega_M = 2\pi \cdot 200\ \text{kHz}$, corresponding to $\tau_M = 1.15\ \text{ns}$, $L_1 = 1\ \text{m}$, $L_2 = 2\ \text{m}$, $L_s = 0.8\ \text{m}$, $\lambda = 10.4\ \text{Å}$.
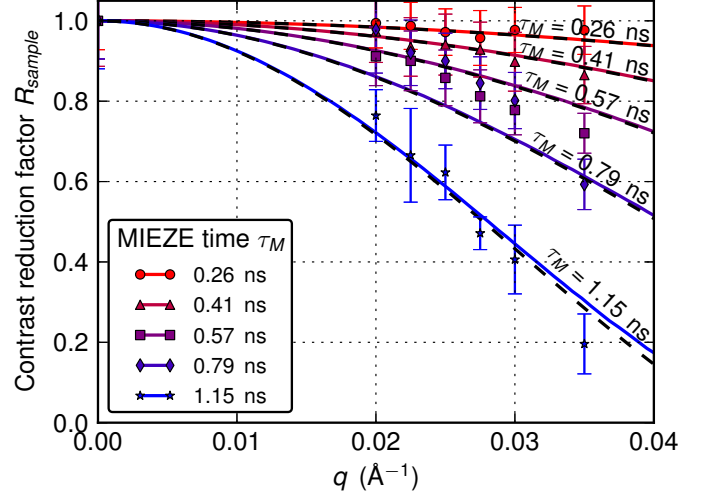

Figure 2: Comparison of the sample reduction factor for a cuboid in fixed geometry showing the reduction factor for the simulation results (solid lines), the analytical results from [12] (dashed lines) and experimental (symbols with error bars) results from the instrument MIRA also performed by [12]. Parameters are as given in [12]: sample width 25 mm, thickness 5 mm, $\lambda = 10.4\ \text{Å}$, ω_M ranges from $2\pi \cdot 46\ \text{kHz}$ to $2\pi \cdot 200\ \text{kHz}$, yielding a MIEZE time τ_M from 0.26 ns to 1.15 ns, respectively. Instrument lengths are: $L_1 = 1\ \text{m}$, $L_2 = 2\ \text{m}$, $L_s = 0.8\ \text{m}$.

We will propose a combined MIEZE/NRSE instrument for measuring slow dynamics, in particular from depolarising samples and samples in extreme environments (magnetic fields, pressure) at the planned European Spallation Source (ESS) in Lund, Sweden. This source will provide neutron pulses with a repetition rate of 14 Hz, a pulse length of 2.8 ms and a total power of 5 MW. The peak intensity will reach 30 times the average intensity of the ILL. A sketch of the planned instrument configuration is shown in Fig. 4. It consists of a beam extraction and guide system based on Montel optics [19, 20, 21, 22], which allows a decoupling of the selection of the size and the divergence of the incident beam. The distance between the focal points of each Montel mirror is projected to be $L_1 = 16\ \text{m}$. The reflecting mirrors are assumed to be 9.6 m long. The goal is to transport only those neutrons to the sample that will be useful for scattering from the sample, i.e. the beam size is equivalent to the sample size and the divergence is such that it is compatible with the requirements of the experiment. All other neutrons are absorbed before, therefore the background will be minimised at the sample position and the low radiation load on the transport system for the neutrons will yield a longer life time of the components.

The chopper system will be designed such that it provides neutrons for wavelength bands $3 \leq \lambda \leq 9.5\ \text{Å}$ and $9 \leq \lambda \leq 15.5$ Å by changing the phase relation between the two choppers. They are located right after the biological shielding of the ESS

(6 m downstream the moderator) and in front of the sample. Therefore, neutrons spanning the whole wavelength band without frame overlap and using all pulses from the moderator are used. The lower wavelength band around 6.25 Å defines the total length of the instrument ($L_{tot} = 45\ \text{m}$) from the moderator to the sample position, which is located 26 m after the biological shielding (Fig. 4).

The coil system consists of two NRSE coils: one in front of the sample and one located between the two Montel mirrors of the guide system. The 16 m long precession region is shielded by μ-metal for providing a zero field region. The first Montel mirror polarises the beam. In front of the sample will be a removable spin analyser. Running the two coils at different RF-frequencies one obtains a time modulated intensity at the detector. Two options are possible:

i. For the small angle scattering regime, a detector of 1 m² with a spatial resolution of 2 mm will be placed 10 m behind the sample allowing a time resolution of the order of µs (see Figs. 6 and 7). Such a detector can be realised for example by combining position-sensitive detectors such as the CASCADE system [16, 17, 18]. It also conserves the MIEZE contrast as described above.

ii. For larger values of q, a set of NRSE coils behind the sample will correct for the path length differences in the beam. Using an analyser bank over an angular range of 90° and a detector distance of 2 m (with a relaxed resolution of 1 cm), this setup will allow for a q-range up to 3 Å⁻¹ with a time resolution exceeding 100 ns. Note that this configuration has not yet been simulated as it needs a different simulation method.
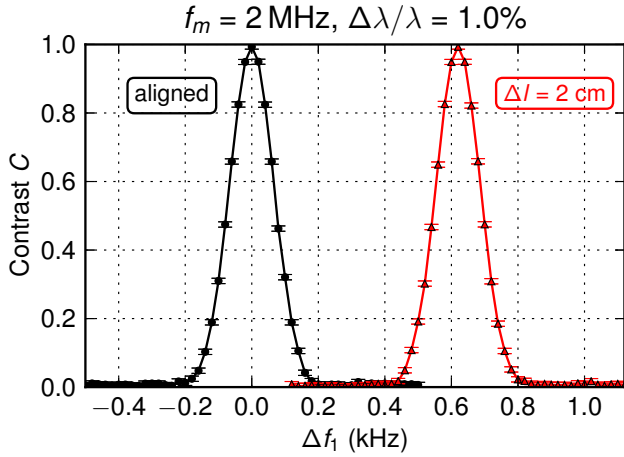
The Monte-Carlo simulations as described in section 3.1

Figure 3: Compensation of a detector offset of 2 cm by adjustment of the first spin flipper frequency. The left curve shows the signal for an aligned detector, the right curve demonstrates that the signal can be recovered for a misaligned detector by changing the frequency $f_M = \omega_M/2\pi$ of the second coil according to Eq. (5). Instrument parameters are: $L_1 = 16\,\mathrm{m}$, $L_2 = 16\,\mathrm{m}$, $L_s = 13\,\mathrm{m}$, $\lambda = 15\,\text{Å}$.
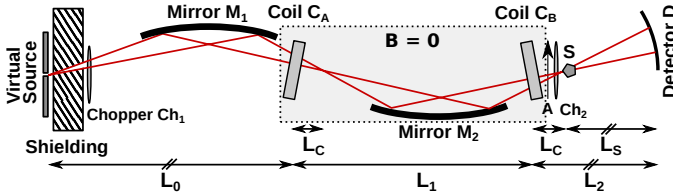

Figure 4: Schematic view of the MIEZE instrument using Montel optics. M_1 and M_2 are reflecting mirrors with a length of 9.6 m each, which is 60% of the distance L_1 between the π-flipper coils C_A and C_B, A and S indicate the analyser and the sample, respectively. The instrument parameters used in the simulations are: Distance from the virtual source with an area of 2 x 2 mm^2 to the coil C_A: $L_0 = 13$ m, distance $L_1 = 16$ m, distance from coil C_B to the detector: $L_2 = 16$ m, distance from coil C_B to the sample: $L_C = 3$ m, distance from the sample to the detector: $L_s = 13$ m.

were now used to simulate the signal for the small angle regime of the proposed instrument i.e. option (i) above. The simulation consists of the ESS source, the instrument including the Montel optics, the MIEZE coils and the detector. Perfect MIEZE coils, Montel mirrors and no gravity were assumed. Note, that the total contrast reduction is obtained by multiplying the individual contrast reductions due to the focusing optics (Fig. 6)) and the sample shape (Fig. 7).

An optimisation of the inclination of the NRSE coils due to the chosen mirror configuration (see Fig. 5) was performed. The influence of the flight path differences on the resolution was significantly reduced for an optimal inclination of the coils by 1.65 degrees. A misplacement of the detectors would degenerate the signal, but can be compensated by the adjustment of the MIEZE frequency as demonstrated in Fig. 3. Using a wavelength of 15 Å and the optimal MIEZE frequency, which allow for maximal MIEZE times of up to a microsecond, the simulation results show no relevant decrease of the MIEZE contrast at
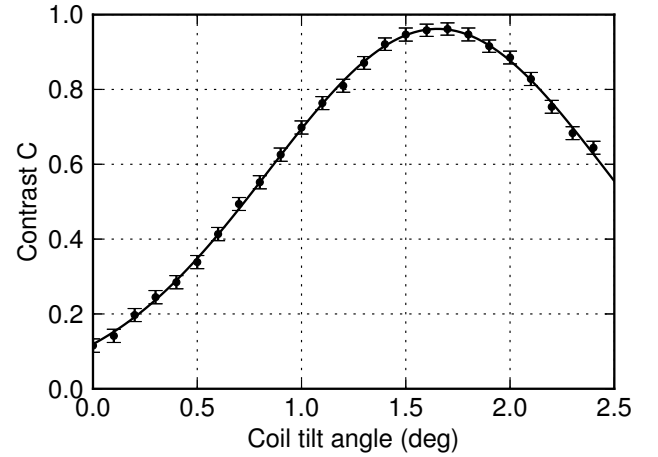

Figure 5: Dependence of the contrast on the tilt of the π-flipper coils. The optimal coil rotation of 1.65^0 is independent of λ.

the optimal inclination of the coils (see Fig. 6). Taking into account the reduction factor due to the sample shape the accessible $q - \tau_M$ space for two typical sample geometries used in the field of magnetism is plotted in Fig. 7. The results demonstrate that the large time resolution up to one microsecond of the instrument can be preserved for selected sample geometries.

In conclusion, we succeeded to prove that Monte-Carlo simulations are a powerful means for the optimisation of spectrometers using the MIEZE technique. Choosing a favourable sample geometry can preserve the excellent time resolution of the instrument. Furthermore, the use of focusing techniques and Montel optics will lead to a low background and a tremendously reduced radiation load on the beam components. Moreover, no mirror optics and no choppers are required inside the biological shielding thus facilitating the maintenance of a MIEZE beam line. Adjusting the MIEZE frequency will compensate for possible detector misplacements. We have shown that path length differences can be effectively compensated by properly tilting the π-flippers in a focussing NRSE/MIEZE instrument.

We have demonstrated that a powerful, low background and low cost MIEZE/NRSE beam line at the ESS can be realised using beam components that are already available now and are in regular use at the beam line RESEDA at FRM II [23] . The time resolution of a MIEZE/NRSE at large angles will be of the same order as for NSE SPAN-like instruments [24]. However, going to small q will add the benefit of performing experiments from depolarising samples and in magnetic fields with a significantly improved time resolution.
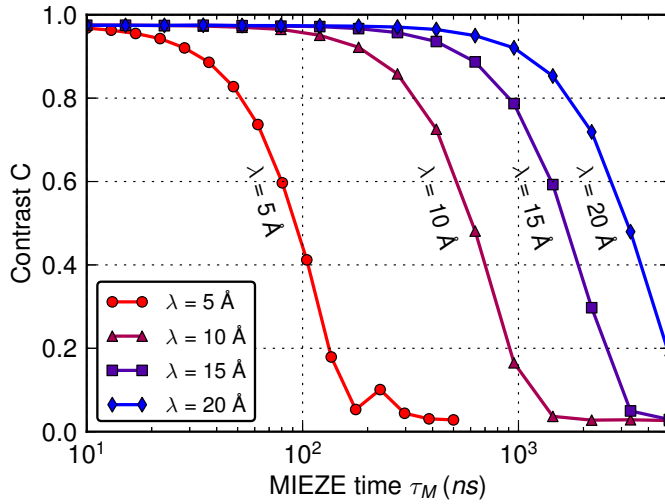
5. Acknowledgements

Figure 6: Contrast vs. MIEZE time τ_M for various wavelengths for the small angle regime without inclusion of the effects of sample shape and gravitation. The instrument parameters are: $L_1 = 16\,\mathrm{m}$, $L_2 = 16\,\mathrm{m}$, $L_s = 13\,\mathrm{m}$. The coating of the Montel optics is $m = 5$ times the critical angle of natural nickel.
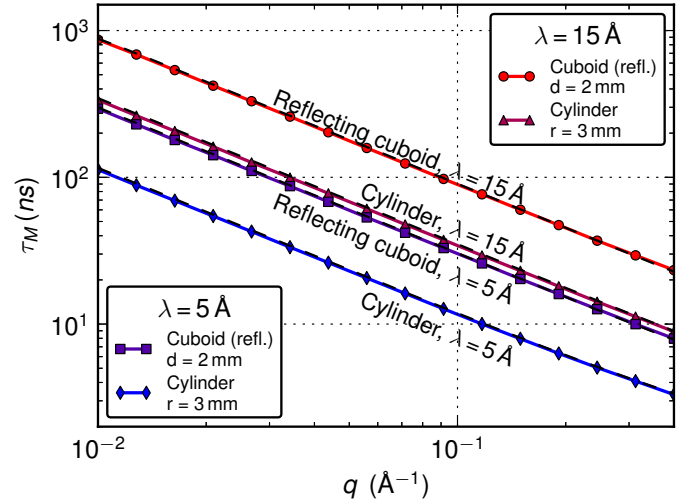

Figure 7: Time resolution limitations from the sample shape, not including effects of the focussing mirrors. The $R = 50\%$ contour for a cuboid sample in reflecting geometry with a thickness of 2 mm (typically used for soft mater) and a cylindrical sample with a radius of 3 mm (typically used for hard condensed matter and for experiments under extreme conditions) are shown for different wavelengths. Instrument parameters are: $L_1 = 16\,\mathrm{m}$, $L_2 = 16\,\mathrm{m}$, $L_s = 13\,\mathrm{m}$.

References

[1] S. Mühlbauer, B. Binz, F. Jonietz, C. Pfleiderer, A. Rosch, A. Neubauer, R. Georgii, P. Böni, Skyrmion Lattice in a Chiral Magnet, Science 323 (5916) (2009) 915–919, doi:10.1126/science.1166767, URL http://www.sciencemag.org/content/323/5916/915.abstract.

[2] W. Münzer, A. Neubauer, T. Adams, S. Mühlbauer, C. Franz, F. Jonietz, R. Georgii, P. Böni, B. Pedersen, M. Schmidt, A. Rosch, C. Pfleiderer, Skyrmion lattice in the doped semiconductor $Fe_{1-x}Co_xSi$, Phys. Rev. B 81 (2010) 041203, doi:10.1103/PhysRevB.81.041203, URL http://link.aps.org/doi/10.1103/PhysRevB.81.041203.

[3] T. Adams, A. Chacon, M. Wagner, A. Bauer, G. Brandl, B. Pedersen, H. Berger, P. Lemmens, C. Pfleiderer, Long-Wavelength Helimagnetic Order and Skyrmion Lattice Phase in Cu_2OSeO_3, Phys. Rev. Lett. 108 (2012) 237204, doi:10.1103/PhysRevLett.108.237204, URL http://link.aps.org/doi/10.1103/PhysRevLett.108.237204.

[4] S. Seki, J.-H. Kim, D. S. Inosov, R. Georgii, B. Keimer, S. Ishiwata, Y. Tokura, Formation and rotation of skyrmion crystal in the chiral-lattice insulator Cu_2OSeO_3, Phys. Rev. B 85 (2012) 220406, doi:10.1103/PhysRevB.85.220406, URL http://link.aps.org/doi/10.1103/PhysRevB.85.220406.

[5] B. Farago, F. Mezei, Study of magnon dynamics in Fe near Tc by modified neutron spin echo techniques, Physica B+C 136 (1–3) (1986) 100 – 102, ISSN 0378-4363, doi:10.1016/S0378-4363(86)80030-4, URL http://www.sciencedirect.com/science/article/pii/S0378436386800304.

[6] L. D. C. Jaubert, P. C. W. Holdsworth, Signature of magnetic monopole and Dirac string dynamics in spin ice, Nature Physics 5 (2009) 258–261.

[7] F. Mezei, Neutron spin echo: A new concept in polarized thermal neutron techniques, Zeitschrift für Physik A 255 (2) (1972) 146–160, doi:10.1007/BF01394523.

[8] R. Gähler, R. Golub, Neutron resonance spin echo, bootstrap method for increasing the effective magnetic field, J. Phys. France 49 (7) (1988) 1195–1202, doi:10.1051/jphys:019880049070119500.

[9] R. Gähler, R. Golub, T. Keller, Neutron resonance spin echo–a new tool for high resolution spectroscopy, Physica B: Condensed Matter 180-181 (Part 2) (1992) 899 – 902, ISSN 0921-4526, doi:10.1016/0921-4526(92)90503-K.

[10] W. Besenböck, R. Gähler, P. Hank, R. Kahn, M. Köppe, C. H. D. Novion, W. Petry, J. Wuttke, First scattering experiment on MIEZE: A fourier transform time-of-flight spectrometer using resonance coils, Journal for Neutron Research 7 (1) (1998) 65–74, doi:10.1080/10238169808200231.

[11] R. Georgii, G. Brandl, N. Arend, W. Häußler, A. Tischendorf, C. Pfleiderer, P. Böni, J. Lal, Turn-key module for neutron scattering with sub-micro-eV resolution, Applied Physics Letters 98 (7) (2011) 073505 – 073505–3, ISSN 0003-6951, doi:10.1063/1.3556558.

[12] G. Brandl, R. Georgii, W. Häußler, S. Mühlbauer, P. Böni, Large scales–long times: Adding high energy resolution to SANS, Nuclear Instruments and Methods in Physics Research A 654 (2011) 394 – 398, doi:10.1016/j.nima.2011.07.003.

[13] P. Willendrup, E. Farhi, K. Lefmann, McStas 1.7 - a new version of the flexible Monte Carlo neutron scattering package, Physica B: Condensed Matter 350 (1–3, Supplement) (2004) E735 – E737, ISSN 0921-4526, doi:10.1016/j.physb.2004.03.193, URL http://www.sciencedirect.com/science/article/pii/S0921452604004144, proceedings of the Third European Conference on Neutron Scattering.

[14] K. Lefmann, K. Nielsen, McStas, a general software package for neutron ray-tracing simulations, Neutron News 10 (3) (1999) 20–23, doi:10.1080/10448639908233684, URL http://www.tandfonline.com/doi/abs/10.1080/10448639908233684.

[15] T. Keller, R. Golub, R. Gähler, Neutron Spin Echo–A Technique for High-Resolution Neutron Scattering, in: R. Pike, P. Sabatier (Eds.), Scattering, Academic Press, London, ISBN 978-0-12-613760-6, 1264 – 1286, doi:10.1016/B978-012613760-6/50068-1, 2002.

[16] C. Schmidt, F. Groitl, M. Klein, U. Schmidt, W. Häußler, CASCADE with NRSE: Fast Intensity Modulation Techniques used in Quasielastic Neutron Scattering, Journal of Physics: Conference Series 251 (1) (2010) 012067, URL http://stacks.iop.org/1742-6596/251/i=1/a=012067.

[17] M. Klein, C. J. Schmidt, "CASCADE, neutron detectors for highest count rates in combination with ASIC/FPGA based readout electronics", Nuclear Instruments and Methods in Physics Research Section A: Accelerators, Spectrometers, Detectors and Associated Equipment 628 (1) (2011) 9 – 18, ISSN 0168-9002, doi:10.1016/j.nima.2010.06.278, URL http://www.sciencedirect.com/science/article/pii/S0168900210014683.

[18] W. Häußler, P. Böni, M. Klein, C. J. Schmidt, U. Schmidt, F. Groitl, J. Kindervater, Detection of high frequency intensity oscillations at RESEDA using the CASCADE detector, Review of Scientific Instruments 82 (4) 045101, doi:10.1063/1.3571300, URL http://link.aip.org/link/?RSI/82/045101/1.

[19] M. Montel, X-ray microscopy with catamegonic roof mirrors, X-ray mi-

croscopy and microradiography, Academic Press, New York, 177–185, 1957.

[20] J. Stahn, T. Panzner, U. Filges, C. Marcelot, P. Böni, Study on a focusing, low-background neutron delivery system, Nuclear Instrum. Methods A 634 (2011) S12.

[21] J. Stahn, U. Filges, T. Panzner, Focusing specular neutron reflectometry for small samples, Eur. Phys. J. Appl. Phys 58 (2012) 11001.

[22] G. E. Ice, J. W. L. Pang, C. Tulk, J. Molaison, J.-Y. Choi, C. Vaughn, L. Lytle, P. Z. Takacs, K. H. Andersen, T. Bigault, A. Khounsary, Design challenges and performance of nested neutron mirrors for microfocusing on SNAP, Journal of Applied Crystallography 42 (6) (2009) 1004–1008, doi:10.1107/S0021889809037595, URL `http://dx.doi.org/10.1107/S0021889809037595`.

[23] W. Häußler, B. Gohla-Neudecker, R. Schwikowski, D. Streibl, P. Böni, RESEDA—The new resonance spin echo spectrometer using cold neutrons at the FRM-II, Physica B: Condensed Matter 397 (2007) 112–114, doi:doi:10.1016/j.physb.2007.02.086.

[24] C. Pappas, G. Kali, P. Böni, R. Kischnik, L. A. Mertens, P. Granz, F. Mezei, Performance of the multidetector NSE spectrometer SPAN at BENSC, Physica B 267-268 (1999) 285–288.